Journal Pre-proof

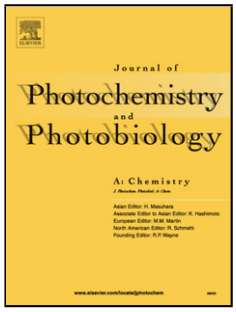

Experimental and theoretical studies of imidazole based chemosensor for Palladium and their biological applications

Shanmugam Suresh, Nanjan Bhuvanesh, Arunachalam Raman, Paramasivam Sugumar, Dhanasekaran Padmanabhan, Shanmugam Easwaramoorthi, Mondikalipudur Nanjappagounder Ponnuswamy, Subbiah Kavitha, Raju Nandhakumar

PII: S1010-6030(19)30682-3

DOI: https://doi.org/10.1016/j.jphotochem.2019.112092

Reference: JPC 112092

To appear in:

Received Date: 22 April 2019

Revised Date: 11 September 2019

Accepted Date: 12 September 2019

Please cite this article as: Suresh S, Bhuvanesh N, Raman A, Sugumar P, Padmanabhan D, Easwaramoorthi S, Ponnuswamy MN, Kavitha S, Nandhakumar R, Experimental and theoretical studies of imidazole based chemosensor for Palladium and their biological applications, *Journal of Photochemistry and amp; Photobiology, A: Chemistry* (2019), doi: https://doi.org/10.1016/j.jphotochem.2019.112092

Experimental and theoretical studies of imidazole based chemosensor for Palladium and their biological applications

Shanmugam Suresh[a], Nanjan Bhuvanesh[a], Arunachalam Raman[b], Paramasivam Sugumar[c], Dhanasekaran Padmanabhan[d], Shanmugam Easwaramoorthi*[,b], Mondikalipudur Nanjappagounder Ponnuswamy [c], Subbiah Kavitha*[,d] and Raju Nandhakumar*[,a]

[a]Department of Chemistry, Karunya Institute of Technology and Sciences (Deemed-to-be University), Karunya Nagar, Coimbatore – 641 114, India. E-mail: nandhakumar@karunya.edu

[b]Inorganic & Physical Chemistry Laboratory, CSIR-Central Leather Research Institute, Adyar, India. Email: moorthi@clri.res.in

[c]Centre of Advanced Studies in Crystallography and Biophysics, University of Madras, Guindy Campus, Chennai 600 025, India.

[d]Department of Biotechnology, Karunya Institute of Technology and Sciences (Deemed-to-be University), Karunya Nagar, Coimbatore – 641 114, India. E-mail: kavibiotec@karunya.edu

Graphical Abstract

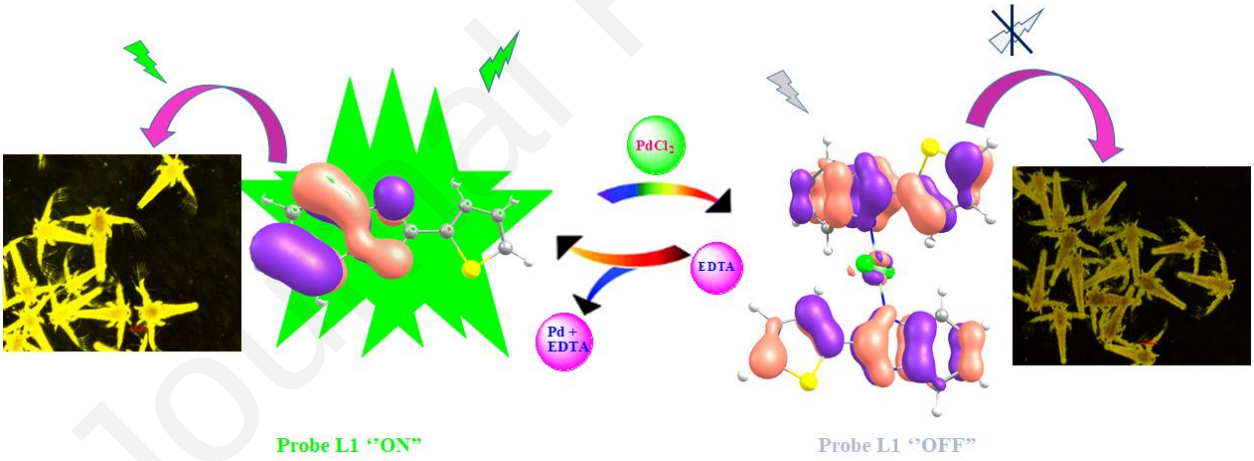

Highlights

- Imidazole derivative bearing a thiphene group (**L1**) senses Pd^{2+} sensor *via* turn on-off mechanism without any influence of other metal ions
- The absorbance intensity of probe **L1** considerably enhanced whereas the fluorescence emission intensity was quenched in the presence of Pd^{2+} ions
- Density Functional Theory (DFT) calculations were used to study the electronic properties
- The intracellular Pd^{2+} ion detection in living cells was performed using probe **L1** on brine shrimp nauplii (*Artemia salina*)

Abstract

An imidazole derivative (probe **L1**) bearing a thiophene group was developed as an ON-OFF fluorescent chemosensor for palladium ions. The UV-Visible absorption and fluorescence spectral behavior of probe **L1** towards various cations were investigated in HEPES buffer aqueous solution. The absorbance intensity of probe **L1** considerably enhanced whereas the fluorescence emission intensity was quenched in the presence of Pd^{2+} ions, while the presence of other metal ions had no notable interference. The stoichiometry of the complex was determined using Job's plot and a plausible recognition mechanism of probe **L1** and Pd^{2+} is proposed. Density Functional Theory (DFT) calculations were used to study the electronic properties and to optimize the structure on the selectivity of Pd^{2+} ions and are correlated with the experimental results. The intracellular Pd^{2+} ion detection in living cells was performed using probe **L1** on brine shrimp nauplii (*Artemia salina*) up to 20 µg/mL**.**

Keywords: Chemosensor, Pd^{2+} ion, colorimetric, fluorescence, DFT, antimicrobial, molecular docking, Bio imaging

1. Introduction

Recently, development of selective and sensitive fluorescent diagnostics for important transition metal ions such as palladium is of huge curiosity due to the plentiful usage in various physical and profitable applications [1-3]. For example, it is extensively used as a catalyst in synthesis because of its brilliant catalytic ability in pharmaceutically valuable products [4,5]. Palladium plays a significant role in the manufacture of medical devices, dental, jewelry, catalytic convertor for automobiles, connecting plating for electronics and as essential catalysts in many organic reactions [6,7]. Palladium can be found in biological materials and augmented by the food chain to cause an imminent fitness problems. After a thorough investigation, World Health Organization (WHO) has confirmed that the deadly dose of palladium is 5-10 ppm, [8–10] and uptake may be controlled to ~ 1.5 – 15 µg/day. Besides the need, palladium causes eye, skin, breathing tract irritation and the complex of Pd (II) are regarded highly toxic and carcinogenic. For example, it can coordinate with bimolecular DNA, proteins consisting of thiol or thiol – ether group containing amino acid, vitamin B6 etc. and are active energy driving centers in living cells [7,11–13]. Analytical instrumentation (plasma emission spectroscopy (e.g. ICP-MS and ICP-AES), atomic absorption spectrometry (AAS), solid phase microextraction-high performance liquid chromatography and X-ray fluorescence) for the quantification of Pd (II) generally costs high price for the instrumentation and tedious complex procedures. Therefore, the development of palladium detecting probes, especially for imaging in living systems and to detect the trace level of the metal remaining in air, water, food product, beverages etc., are in high demand. Nevertheless, there are some reported analytical methods for the recognition of Pd^{2+} ion; however, fluorescent based detection has great attention due to its extreme sensitivity and selectivity and to some extent suitability to be active in biological samples. As a consequence, development of fluorescent chemosensors for palladium ion is highly needed. We herein report a heterocycle based small molecule, imidazole thiophene conjugate **L1** coupled by a freely rotatable carbon-carbon single bond for the selective detection of palladium. To the better of our understanding this is the first report where there is an absorption enhancement and emission quenching during the sensing of palladium by the chemosensor **L1** as a dual mode detection method in semi aqueous media. In addition, imidazole based compounds play an important role as anticancer, antifungal, antibacterial and anti-inflammatory agents [14–16]. Hence, the chemosensor **L1** and its palladium complex are further screened for various biological applications including bio-imaging of *Artemia Salina*.

2. Experimental

2.1. Materials & Instruments

All the chemicals and reagents such as 1,2-phenylenediamine, thiophene-2-carboxaldehyde, absolute ethanol, sodium hydroxide, high pure HEPES (99.0 %), Na_2EDTA (98.0%) etc., were purchased from commercially available sources like Himedia, Loba Chem. Ltd., Sigma Aldrich etc., were used after being purified by standard techniques. TLC plates were purchased from Merck pre-coated alumina (Aluminium oxide) sheets of 60 F-254. Melting point was recorded using a Buchi Melting Point B-545, an electrothermal apparatus using capillary tubes and are uncorrected. The nitrate, acetate and chloride salts of K^+, Ca^{2+}, Na^+, Mg^{2+}, Cr^{3+}, Mn^{2+}, Co^{2+}, Ni^{2+}, Cu^{2+}, Hg^{2+}, Cd^{2+}, Fe^{3+}, Zn^{2+}, Al^{3+}, La^{2+}, Bi^{3+}, Sr^{2+}, Ag^+, Ba^{2+}, Zr^{2+}, Pb^{2+}, Fe^{2+}, Ce^{3+} and Pd^{2+} were used as metal salts for recognition. EDTA solution was prepared with ethylenediaminetetraacetic acid disodium salt (Na_2EDTA) (100 equiv.) in double distilled water (25 mL). Double distilled water was prepared in the laboratory using a water treatment device and used throughout the work. ^1H NMR and ^{13}C NMR spectra were verified on a Bruker 400 and 100 MHz high-resolution NMR spectrometer, respectively, utilizing DMSO-d_6 solution with TMS as an internal standard and coupling constants (J) were measured in Hertz. LC-MS and ESI mass were determined on a Shimadzu Lab Solutions Data Report. UV-Visible absorption spectrum was taken at ambient temperature using a Shimadzu UV-Vis spectrophotometer using 1 cm path length quartz cuvette. Fluorescence emission spectra were recorded on a Jasco FP-8200 spectrofluorometer with quartz cuvette 4.5 cm height of 1 cm path length. The excitation and emission slot widths recorded were 5.0 nm. All cation absorption and emission spectra were recorded at 24±1°C. Scanning Electron Microscopy (SEM) images and EDAX spectrum were carried out using SEM instrument (Model: JOEL-6390, Japan) whereby the samples are dispersed on a carbon tape. Docking calculations were done using Docking Server (Bikadi, Hazai, 2009), needed hydrogen atoms, Kollman charges, and solvation parameters were added with AutoDock tools.[17] Molecular docking simulations were performed using the Lamarckian genetic algorithm (LGA) and the Solis & Wets local search technique.[18]

2.2. Synthesis of 2- (thiophen-2-yl)-1*H*-benzo [*d*] imidazole (Probe L1)

To a stirred of *o*-phenylenediamine in 10 mL absolute ethanol (0.50 g, 0.005 mol), 2-thiophene carboxaldehyde (0.57 g, 0.005mol) in absolute ethanol (20 mL) was added slowly. The reaction mixture was further stirred under room temperature for 8 hrs. After completion of the reaction, monitored by the TLC, the yellow precipitate formed was filtered and washed several times with cold ethanol. Finally, recrystallization of the crude product from ethanol gave the probe **L1** in 80% yield. Mp: 152 ^{0}C; ^{1}H NMR (400 MHz, DMSO-d_6): δ (ppm): 12.96 (s, 1H), 7.84-7.83 (d, 1H), 7.73-7.72 (d, 1H), 7.55 (s, 1H), 7.24-7.18 (m, 3H) (Figure S1). ^{13}C NMR (100 MHz, DMSO-d_6): 147.5(1C), 134.18(2C), 129.2(2C), 128.7(2C), 127.1(2C), 122.66(2C) (Figure S2). LC-MS (ESI) m/z calcd. For $C_{11}H_8N_2S^+$ (M) 200.26, found 199.726 (M-1) (Figure S3). (**Scheme 1**).

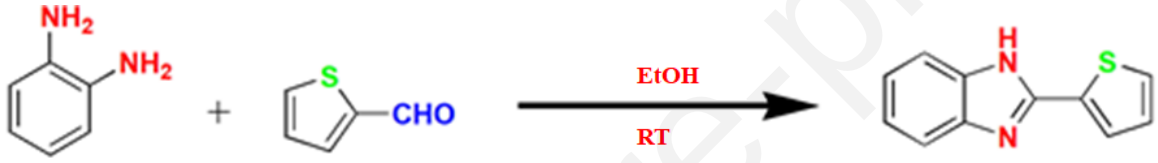

Scheme 1: Synthesis of probe **L1**. Absolute Ethanol, RT, 8 hours

2.3. UV- Visible and fluorescence studies

The UV-Visible and the fluorescence spectra of the chemosensor **L1** were recorded at 25 °C in CH_3CN/H_2O (1:1 v/v) using 50 mM HEPES buffer at a physiological pH of 7.4. Stock solutions of the metal ions utilized for the study was prepared (2×10^{-3} M concentration of probe **L1** (CH_3CN/H_2O (1:1 v/v)), HEPES=50 mM, pH=7.4) prior to the experiment. The solutions of metal ions were prepared from nitrate salts of Ag^+, Al^{3+}, Ba^{2+}, Ca^{2+}, Cd^{2+}, Ce^{3+}, Co^{2+}, Cr^{3+}, Cu^{2+}, Fe^{2+}, Fe^{3+}, Hg^{2+}, K^+, La^{3+}, Li^+, Mg^{2+}, Mn^{2+}, Na^+, Ni^{2+}, Pb^{2+}, Sr^{2+}, Zn^{2+}, Pd^{2+} and Zr^{2+}.

2.4. Density Functional Theory (DFT) calculation

The molecular geometry optimization with respect to energy was investigated computationally by performing Density Functional Theory (DFT) to get way for validation of experimental results. The ground state geometries of probe **L1** and probe **L1**+Pd^{2+} were optimized using Density Functional Theory (DFT) with B3LYP functional and 6-31G (d) basis set using Gaussian 09 program. To verify the stoichiometric ratio and stability of probe **L1** and its complex with Pd^{2+}, optimized geometry parameters such as ground state energies, bond length, bond angles, etc., were calculated.

2.5. Anti-bacterial activity

Anti-bacterial activity of the **L1**, and **L1**+Pd^{2+} were tested against the cultures of *Staphylococcus aureus* and *Escherichia coli* by agar well diffusion method [19–21] using Muller-Hinton Agar (MHA). Sterile cotton swab was dipped in the respective broth culture and squeezed against the wall of the tube to drain excess liquid. Then it was swabbed on to the surface-dried MHA plates. Wells (4-6 mm) were made using a sterile cork borer (4 wells/plate; each for **L1**, Pd^{2+}, **L1**+Pd^{2+} and DMSO a separate plate was used for Ampicillin; 1 plate per bacteria). 50 µL of each mixture was added to the respective wells, allowed to be absorbed for 20-30 minutes at 4°C and thereafter hatched at 37 °C for 18-24 hours. Diameter of zone of inhibition (in mm) was measured and tabulated. Briefly, a single colony was used to inoculate 10 mL of Mueller-Hinton broth (Himedia laboratories, Mumbai, India) and incubated overnight at 37 °C. From this overnight culture broth, 0.1% inoculum (10 µL) was used to inoculate a fresh Muller-Hinton broth (10 mL) and incubated at 37°C until the turbidity of the cultures were visually equivalent to that of the 0.5 MacFarland Standard tube (To prepare 10 mL of this standard solution, 0.05 mL of 1% Barium chloride was added to 9.95 mL of 1% Sulphuric acid and mixed well to uniform turbidity. The absorbance of 0.5 McFarland Standard gives an absorbance in the range of 0.08 to 0.1 at 625 nm). This gives an approximate bacterial suspension equal to 1.5 x 10^8 CFU/ mL. Hence, the probe **L1**, Pd^{2+}, and **L1**+Pd^{2+} were dissolved in dimethyl sulphoxide (DMSO) at a concentration of 0.1 g/mL (10%), with DMSO and the antibiotic ampicillin (200 µg/mL) acting as controls.

2.6. Docking Studies

Docking calculations were carried out using Docking Server[22]. Gasteiger partial charges were added to the ligand atoms. Non-polar hydrogen atoms were merged and rotatable bonds were defined. Docking calculations were carried out on Untitled-1 protein model. Essential hydrogen atoms, Kollman united atom type charges, and solvation parameters were added with the aid of AutoDock tools. Affinity (grid) maps of 60×60×60 Å grid points and 0.375 Å spacing were generated using the Autogrid program. AutoDock parameter set- and distance-dependent dielectric functions were used in the calculation of the van der Waals and the electrostatic terms, respectively. Docking simulations were performed using the Lamarckian genetic algorithm (LGA) and the Solis & Wets local search method. Initial position, orientation, and torsions of the ligand molecules were set randomly. All rotatable torsions were released during docking. Each docking experiment was derived from 10 different runs that were set to terminate after a maximum of 250000 energy evaluations. The population size was set to 150. During the search, a translational step of 0.2 Å, and quaternion and torsion steps of 5 were applied.

2.7. Epifluorescence chemosensor analysis of *Artemia Salina*

Bio-probing potential of probe **L1** was performed on *Artemia Salina* as described earlier [23] with little modification. In brief 10-12 hrs post-hatched active nauplii were selected based on active movement under illumination and transferred to polypropylene PCR tube contain 50 uL of brine solution (3.5 % NaCl w/v), 20 uL of 4 $\times 10^{-5}$ of probe **L1** in CH_3CN/H_2O (1:1 v/v) pH = 7.4 used as ligand control, 20 µL of Pd^{2+} ions in100 equiv.CH_3CN/H_2O (1:1 v/v) served as metal control, Probe **L1**+Pd^{2+} (1:1) 20 µL was added to study the metal ligand interaction. 50 mM HEPES buffer at 25^{o} C were used to make up the final volume of 50 uL in all the experiment tubes, 50 uL of PBS buffer served as experimental control, CH_3CN as solvent control. All the tubes incubated for 60 minutes.at room temperature and washed with 1× PBS post incubation to remove the unbound **L1** and Pd^{2+} and emission were recorded using Nikon Eclipse TS100 Epifluorescence microscopy attached with Red and green filter.

3. Results and Discussion

The single step condensation product of *o*-phenylenediamine and 2-thiophene carboxyaldehyde in absolute ethanol yielded the desired chemosensor **L1.** The synthesized chemosensor **L1** was validated with the help of ^{1}H-NMR, ^{13}C–NMR, and LC-MS spectroscopic techniques. The probe **L1** was dissolved in acetonitrile: water (1:1) and scanned in wavelength range 200-800 nm for UV-Visible absorption spectra plot. In order to consider the Pd^{2+} recognition abilities of the sensor, we carried out a serious of Host-Guest recognition experiments in CH_3CN/H_2O for UV-Visible absorption and fluorescence emission studies. The probe **L1** showed a rapid enhancement in absorbance in the presence of Pd^{2+} ion. At the same time, the fluorescence emission of probe **L1** was quenched [24]. The absorbance and fluorescence emission of probe **L1** in acetonitrile/water solution are illustrated in Figure 1.

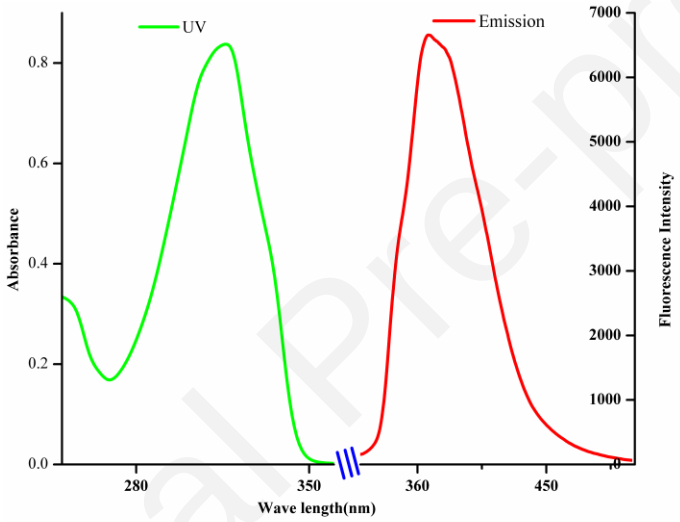

Figure 1. UV-Visible absorption (2×10^{-5} M) and fluorescence spectra (10 µM) of probe **L1** in CH_3CN/H_2O (1:1 v/v) pH = 7.4 using 50 mM HEPES buffer solution at 25 °C.

3.1 Selectivity of metal ions by UV-Visible Absorption studies

The UV-Visible absorption spectra of probe **L1** was investigated in acetonitrile/water at an ambient temperature. The solution of probe **L1** (2×10^{-5} M) in CH_3CN/H_2O [(1:1 v/v) pH = 7.4 using 50 mM HEPES buffer solution at 25 °C] was colorless and exhibited an absorption peak at 320 nm due to the π-π^* transition. The sensing ability of probe **L1** was investigated by adding various cations, such as Zr^{2+}, Pb^{2+}, Zn^{2+}, Co^{2+}, Ni^{2+}, Ca^{2+}, Mn^{2+}, Cr^{3+}, Ba^{2+}, Ce^{3+}, Mg^{2+}, Fe^{2+}, Fe^{3+}, Bi^{3+}, Sr^{2+}, Ag^{+}, La^{2+}, K^{+}, Al^{3+}, Cu^{2+}, Cd^{2+}, Hg^{2+}, Na^{+} and Pd^{2+} to sensor **L1** by UV

spectroscopic method. While adding Pd^{2+} ion to probe **L1,** there was an enhancement in the absorption peak with a notable blue shift from 320 nm to 310 nm in the UV-Visible absorption spectrum and the colorless solution turned to pale yellow (Figure 2). At the same time there were no significant changes in the absorption spectra during the addition of other cations such as Zr^{2+}, Pb^{2+}, Zn^{2+}, Co^{2+}, Ni^{2+}, Ca^{2+}, Mn^{2+}, Cr^{3+}, Ba^{2+}, Ce^{3+}, Mg^{2+}, Fe^{2+}, Fe^{3+}, Bi^{3+}, $Sr^{2+,}$ Ag^{+}, La^{2+}, Al^{3+}, Cu^{2+}, Cd^{2+}, Hg^{2+}, Na^{+} and K^{+} to solution of sensor **L1.** Hence the chemosensor **L1** selectively detects Pd^{2+} ion compared to other cations.

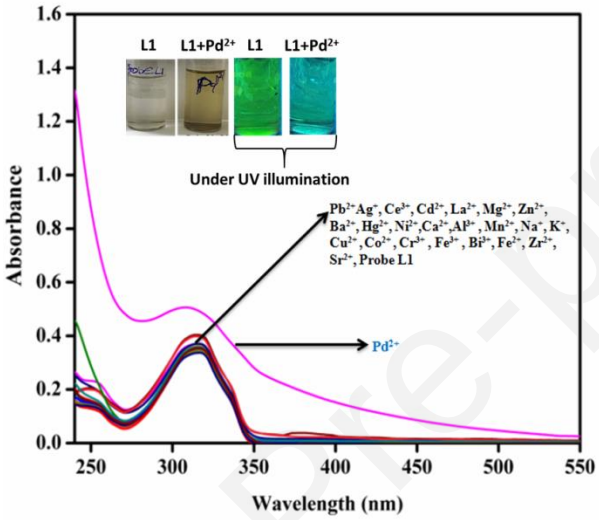

Figure 2. Absorbance spectra probe **L1** (2×10^{-5} M) in the presence of various metal ions in CH_3CN/H_2O solution (1/1 v/v, HEPES 50 mM, pH=7.4). (Inset: naked eye colour change and under UV illumination of probe L1 and L1+Pd^{2+})

3.2 Selectivity of metal ions by emission studies

The emission spectra of probe **L1** towards the selectivity of metal ions such as the nitrate and chloride salts of Na^{+}, K^{+}, Al^{3+}, Cu^{2+}, Cd^{2+}, Hg^{2+}, Zr^{2+}, Pb^{2+}, Zn^{2+}, Co^{2+}, Ni^{2+}, Ca^{2+}, Mn^{2+}, Cr^{3+}, Ba^{2+}, Ce^{3+}, Mg^{2+}, Fe^{2+}, Fe^{3+}, Bi^{3+}, $Sr^{2+,}$ Ag^{+}, La^{2+} and Pd^{2+} in CH_3CN/H_2O (1/1 (v/v) HEPES = 50 mM, pH=7.4 solution excited at 320 nm were recorded and analyzed. On the addition of various metal ions (100 equiv.) to chemosensor **L1,** there was a decrease in fluorescence intensity at 370 nm for all the metal ions except for Pd^{2+} ions**.** Nevertheless, during the addition of Pd^{2+} ions to the chemosensor **L1**, the fluorescence intensity was drastically quenched,[25],[26] suggesting that the probe explicitly recognize Pd^{2+} ions over other cations.

This observation clearly indicates that the probe **L1** which showed an intense fluorescence before the addition of Pd^{2+} ion, was quenched[27],[28] after the addition of Pd^{2+} ion (Figure 3a). [29]

3.3 Effect of Counter anions

The effect of the counter anions on the selectivity of Pd^{2+} ions was then studied which is shown in Figure 3b. Accordingly, three types of palladium salts were taken i.e. $Pd(NO_3)_2$, $PdCl_2$ and $Pd(OAc)_2$ and added with the probe **L1** in CH_3CN/H_2O solution (1/1 v/v, HEPES 50 mM, pH=7.4), excited at 320 nm. For all the three salts, the fluorescence intensity was quenched during the addition of the probe **L1**. These results indicate that the selectivity depends on the palladium ion ruling out the counter anion effect.

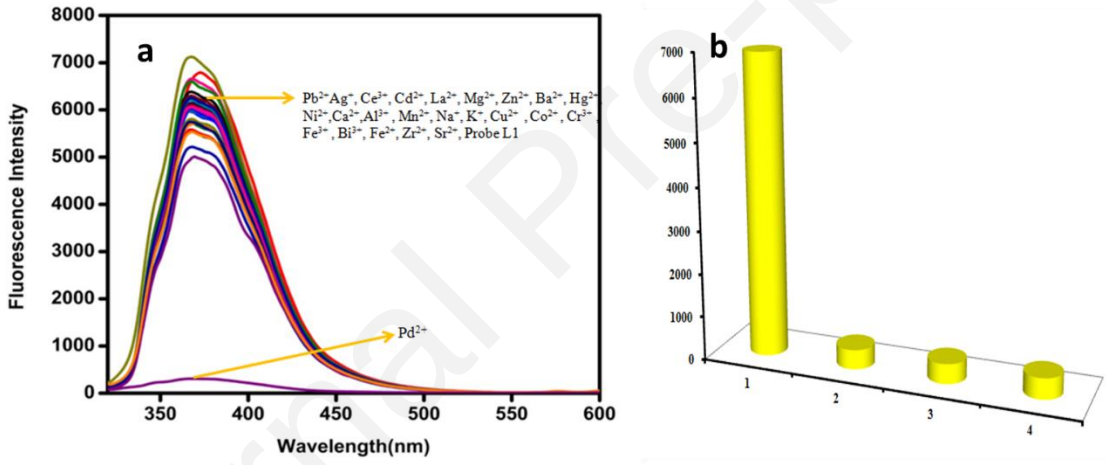

Figure 3. (a) Fluorescence emission spectral changes of probe **L1** (10 µM) in CH_3CN/ H_2O solution (1/1 v/v, HEPES 50 mM, pH=7.4) (excitation at 320 nm) a) in the presence of various metal ions. b) Different counter ions 1. Probe **L1**, 2. Probe **L1**+ Pd $[(NO)_3]_2$, 3. Probe **L1** + $PdCl_2$, 4. Probe **L1** + Pd $(OAc)_2$

3.4 Anti-jamming experiments

To further check the possibility of interference of other metal ions during the Pd^{2+} ion detection by the probe **L1**, anti-jamming experiments were performed by utilizing the absorption spectroscopic technique**.** Accordingly, the ability of receptor **L1** to detect Pd^{2+} ion was measured

utilizing 100 equiv. Pd^{2+} ion with equivalent proportion including Na^{+}, K^{+}, Al^{3+}, Cu^{2+}, Cd^{2+}, Hg^{2+}, Zr^{2+}, Pb^{2+}, Zn^{2+}, Co^{2+}, Ni^{2+}, Ca^{2+}, Mn^{2+}, Cr^{3+}, Ba^{2+}, Ce^{3+}, Mg^{2+}, Fe^{2+}, Fe^{3+}, Bi^{3+}, $Sr^{2+,}$ Ag^{+}, and La^{2+}. There were no obvious changes in the fluorescence intensity with all the metal ions, which suggest that the probe **L1** can be utilized for detection of Pd^{2+} ion in biological and environmental samples. (Figure 4).[30,31]

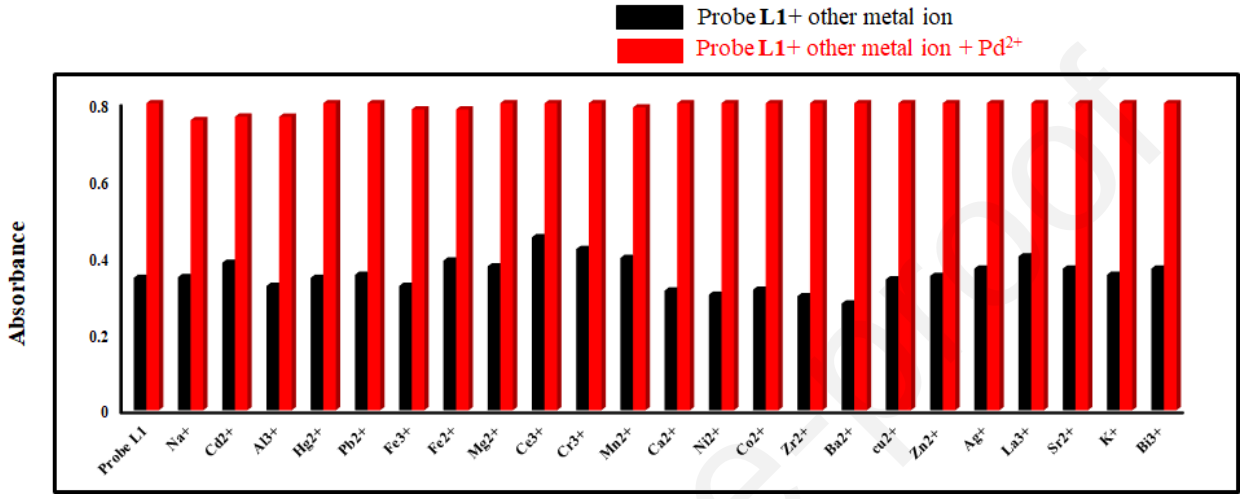

Figure 4. Relative absorbance analysis of probe **L1** (2×10^{-5} M) in CH_3CN/H_2O solution (1/1 v/v, HEPES 50 mM, pH=7.4) with different competing metal ions (100 equiv.) in the absence and presence of Pd^{2+}. Black bar represents the absorbance of probe **L1** with 100 equiv. of other metal ions. Red bar represents the absorbance changes during the addition of 100 equiv. of different relevant competing metal ions to the solution containing the probe **L1** and Pd^{2+}

Similarly, another experiment was conducted utilizing the fluorescence technique as shown in Figure 5. The fluorescence spectral changes of sensor **L1** was measured by the treatment of 100 equiv. Pd^{2+} ions in the presence of same equiv. of other interfering metal ions including Na^{+}, K^{+}, Al^{3+}, Cu^{2+}, Cd^{2+}, Hg^{2+}, Zr^{2+}, Pb^{2+}, Zn^{2+}, Co^{2+}, Ni^{2+}, Ca^{2+}, Mn^{2+}, Cr^{3+}, Ba^{2+}, Ce^{3+}, Mg^{2+}, Fe^{2+}, Fe^{3+}, Bi^{3+}, $Sr^{2+,}$ Ag^{+}, and La^{2+}. These tested interfering metal ions showed no significant interference with the detection of Pd^{2+} ions. Therefore, sensor **L1** could be used for the detection of Pd^{2+} ions as a dual mode detection which includes both the absorption as well as emission techniques with enhancement and quenching respectively.[32],[33]

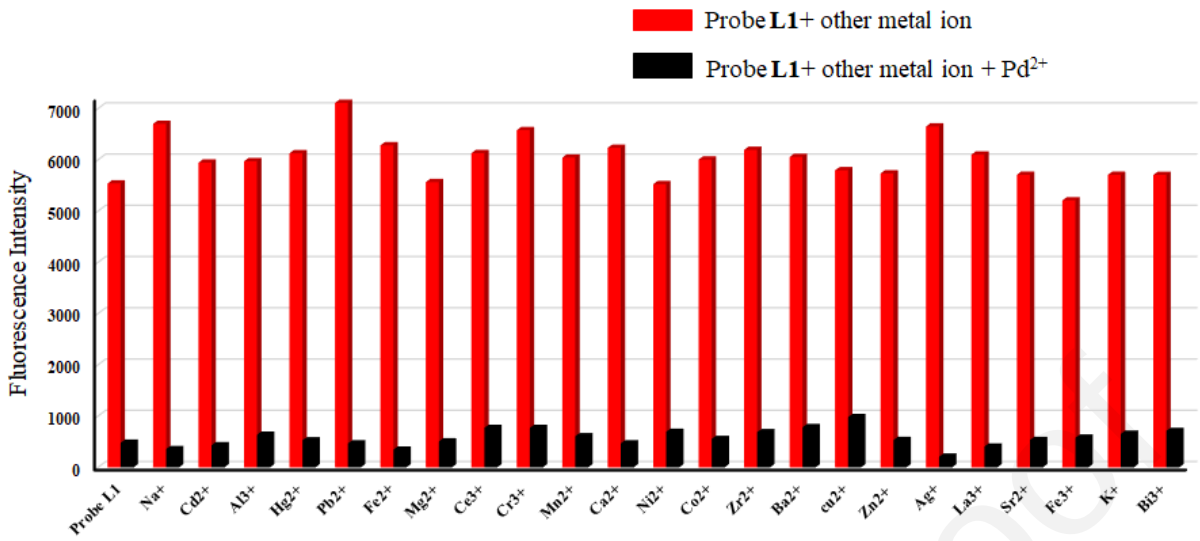

Figure 5. Relative fluorescence intensities of probe **L1** (10μM) in CH_3CN/H_2O solution (1/1 v/v, HEPES 50 mM, pH=7.4) and then with addition of different metal ions to 100 equiv. Pd^{2+}. Red bar represents the emission intensity of probe **L1** with 100 equiv. other metal ions. Black bar represents the florescence changes during the addition of 100 equiv. of different relevant competing metal ions to the solution containing the probe **L1** and Pd^{2+} (100 equiv.).

3.5 Binding analysis of probe L1 with Pd^{2+}

A further understanding of the sensing behaviour of probe **L1** to Pd^{2+}, absorption titration experiment was done by the incremental addition of various amounts of Pd^{2+} ions to a solution of **L1**. As shown in Figure 6, an increase in the absorbance intensity was observed with increasing Pd^{2+} concentration (0-50 equiv.). However, the absorbance spectral changes were almost saturated upon addition of 50 equiv. of Pd^{2+}, revealing that **L1** interacts with Pd^{2+} in 2:1 stoichiometry.[34] During the titration procedure, there was a notable shift of the absorbance peak intensity from 320 nm to 310 nm (blue shift), indicating the possibility of an intramolecular charge transfer (ICT) between the imidazole scaffold and thiophene moiety.

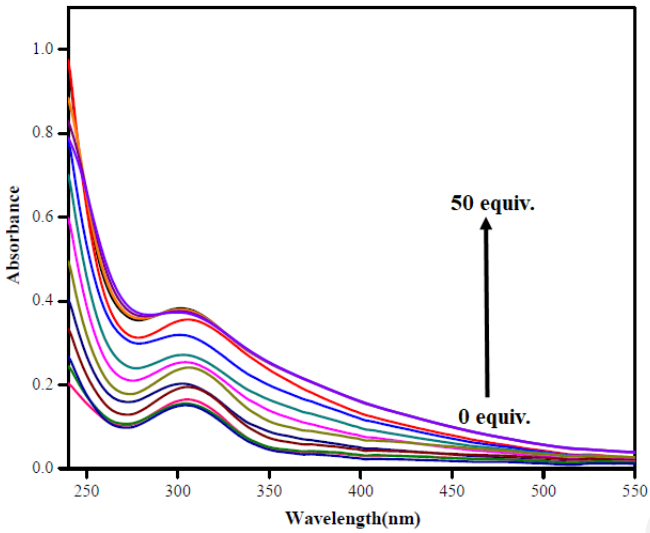

Figure 6. UV- visible absorption spectra of probe **L1** (2×10^{-5} mM) (CH_3CN/H_2O, v/v, 1/1, HEPES, pH- 7.4) upon addition of different amount of Pd^{2+} (0-50 equiv.)

Next, a similar titration profile was carried out between the probe **L1** and Pd^{2+} ion using the fluorescence technique as shown in Figure 7**.** Accordingly, the fluorescence titration of sensor **L1** with Pd^{2+} ion was investigated in CH_3CN: H_2O solution (1:1 v/v, HEPES 50 mM, pH=7.4). The titration clearly indicates that the fluorescence emission intensity at 370 nm gradually decreases as the concentration of Pd^{2+} ion increases. The titration gets saturated during the addition of 28 equivalents of Pd^{2+} ions to probe **L1**. [35,36]

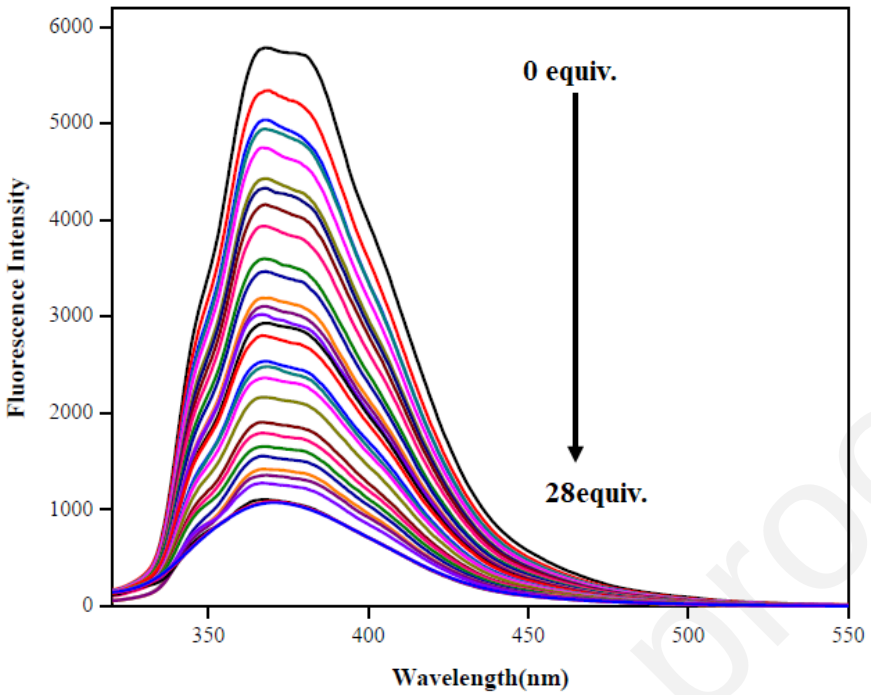

Figure 7. Fluorescence titration of **L1** (2×10^{-5} M) with Pd^{2+} ion (0-28 equiv.) in CH_3CN/ H_2O solution (1:1 v/v, HEPES 50 mM, pH=7.4).

Furthermore, the solubility of the probe **L1** and the impact on the absorption and emission spectra were measured by using different proportions of water and acetonitrile. There was a gradual increase of intensity at 320 nm and 370 nm in both absorbance and emission spectra respectively, as the portion of water rises (f_w) from 0 to 100%. [37–39] However, there was precipitate formation occurred after the (1:1) mixture of acetonitrile/water. Therefore, the (1:1) mixture of acetonitrile/water mixture was selected for all the experiments. In addition, absence of any spectral shift indicates that there was no aggregation induced emission occurring in the probe **L1.** (Figure 8(a) (b))

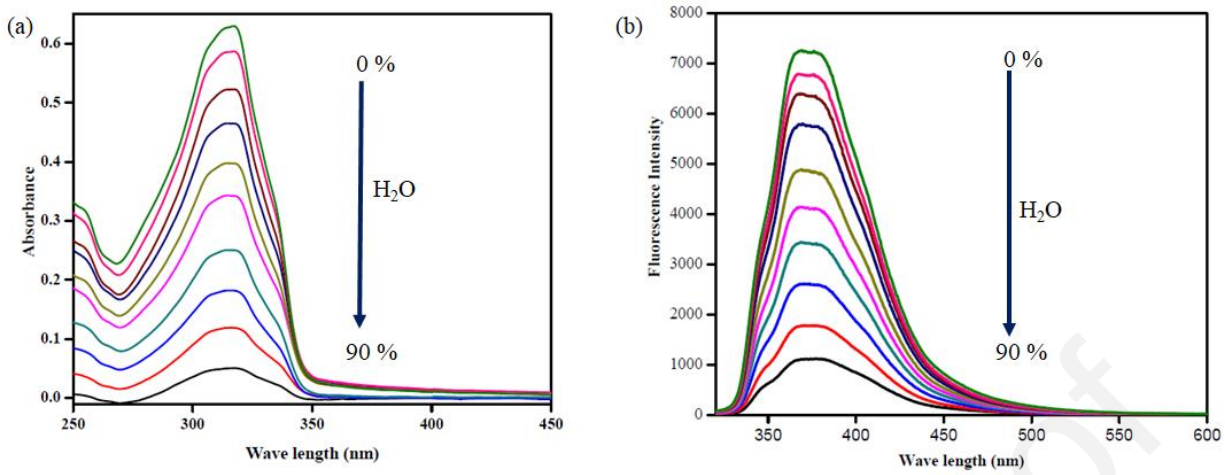

Figure 8. (a) UV-Visible absorption and (b) Fluorescence emission spectra (λ_{em}–370 nm) of probe **L1** (CH_3CN: H_2O system with different water fraction solution).

3.6 Job's plot and association constant analysis

To explore the binding mode between **L1** and Pd^{2+} (Host-Guest) complex through absorption studies, binding analysis were carried out by the Job's plot method (Figure 9(a)). The complex showed a maximum mole fraction of **L1** is 0.3 at 310 nm, which established a 2:1 (**L1**: Pd^{2+}) binding stoichiometry. The binding stoichiometry between **L1**: Pd^{2+} was further confirmed by the Benesi–Hildebrand nonlinear curve fitting method as shown in (Figure 9(b)). The association constant was determined to be Ka = 1.27 x 10^4 M^{-1} for the **L1**: Pd^{2+} complex. The 2:1 stoichiometry was further confirmed by LC-MS as shown in the Supporting Information (Fig. S4). A peak at m/z 542, which corresponds to [2 **L1**+ Pd + Cl]$^+$ was clearly observed in the LC-MS. The limit of detection of **L1** is found to be 13.3 ×10^{-6} mol L^{-1}, which is calculated using 3δ/S, where δ was the standard deviation of the blank signal, and S was the slope of the linear calibration plot.

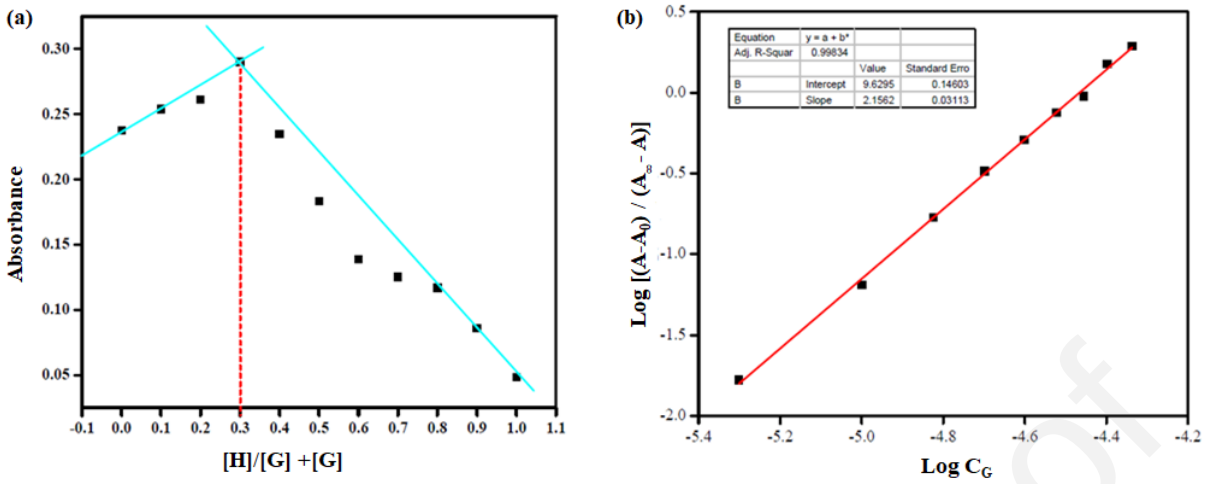

Figure 9. (a) Job's plot of a 2: 1 complex of Pd^{2+}, where the absorbance at 310 nm was plotted probe **L1** (2×10^{-5} M) against the mole fraction of Pd^{2+} (100 equiv.) acetonitrile: water (1:1 v/v, 50mM HEPES buffer) solution. (b) Benesi-Hildebrand plot of probe **L1** with Pd^{2+} ions was in acetonitrile: water (1:1 v/v, 50 mM HEPES buffer) solution.

Similarly the quenching effect of probe **L1** during the addition of Pd^{2+} ions and their binding studies using the fluorescence technique were calculated using the Job's plot method [40]. The complex showed a maximum mole fraction of **L1** is 0.3 which established a 2:1 (**L1**:Pd^{2+}) binding stoichiometry (Figure 10(a)). The binding stoichiometry between **L1**:Pd^{2+} was further confirmed by the Benesi–Hildebrand nonlinear curve fitting method (Figure 10(b)). The association constant was determined to be 1.84×10^{4} M^{-1} for the **L1**:Pd^{2+} complex. The detection limit was found to be 1.53×10^{5} M^{-1} .[41,42]

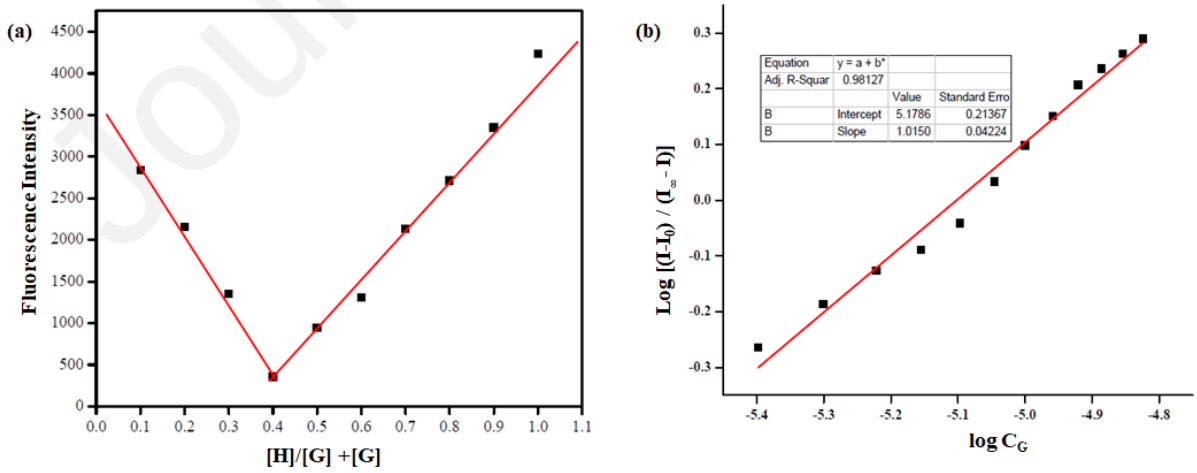

Figure 10. (a) Job's plot of a 2: 1 complex of Pd^{2+}, where the emission at 370 nm was plotted against the mole fraction of Pd^{2+}. (b) Benesi- Hildebrand plot of probe **L1** with Pd^{2+} ions in an acetonitrile: water (1:1 v/v, 50mM HEPES buffer) solution.

Furthermore, ^{1}H NMR analysis were performed to corroborate the coordination structures for Pd^{2+} complex with **L1** in a DMSO-d_6. (Figure 11) shows the partial ^{1}H NMR spectra of **L1** measured in a DMSO-d_6 with and without Pd^{2+} (0-1 equiv). All chemical shifts were identified by $^{1}H-^{1}H$ COSY analysis (Figure 12& 13). Addition of Pd^{2+} leads to a large downfield shift of the thiophene-benzimidazole protons (H_a, H_b, H_c, H_d, H_e, H_f, H_g,). These changes in the chemical shift value of aromatic protons are due to the decrease in electron density of the thiophene-benzimidazole moieties by the benzimidazole N coordination. The disappearance of the NH peak after the addition of palladium may be due to the replacement of exchangeable proton with deuterium.This indicates that there is a possible Pd^{2+} coordination with the benzimidazole 'N' as shown in scheme 2.

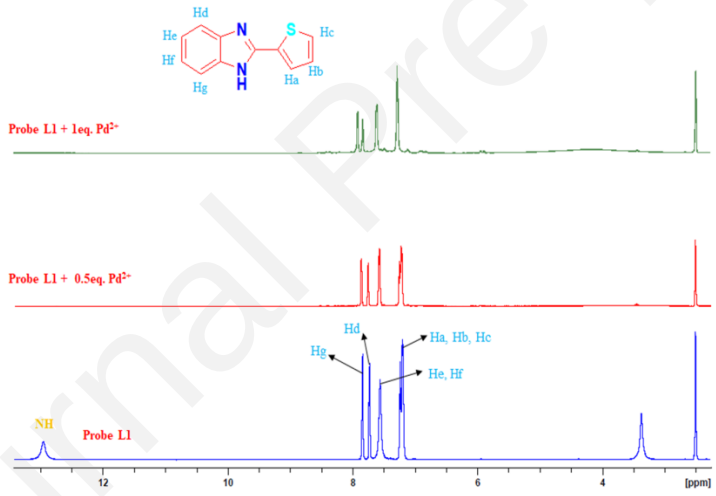

Figure 11. ^{1}H- NMR (400 MHz) titration of probe **L1** (blue line spectra), probe **L1**+ 0.5 equiv. Pd^{2+} (red line spectra), probe **L1**+ 1.0 equiv. Pd^{2+} (green line spectra) in DMSO-d_6.

3.7 Effect of pH, time and reversibility

For practical applicability of fluorescent probes, the effect of pH and time plays a vital role in the selectivity of metal ions. Hence, the same was investigated with probe **L1** detecting Pd^{2+} ions by fluorescence technique, at different pH levels in CH_3CN/H_2O (1/1 v/v) solution.

The pH was adjusted using 10 mM of NaOH and HCl solutions in double distillated water. The result showed that the probe **L1** displays a strong fluorescence a variety of pH range except a strong enhancement between 3 and 5 pH ranges under acidic conditions. Similarly, **L1**-Pd^{2+} complex also gave the same fluorescence intensity except quenching in the detection process. (Figure S8 (top panel)). Therefore, the physiological pH of 7.4 was selected as the working condition through the spectroscopic experiments. The time taken for complete quenching of Pd^{2+} ion by probe **L1** in CH_3CN/H_2O (1/1, v/v) buffered at pH = 7.4 (50mM) is shown in Figure S8 (b). The result clearly indicates that the detection of Pd^{2+} ions by the probe **L1** is completed within two minutes and remained steady for further on hour. Hence, probe **L1** can be utilized to detect Pd^{2+} ions in a short span of time.

The reversibility of **L1** to Pd^{2+} was demonstrated by adding EDTA into a mixture of **L1** and Pd^{2+} (Figure S9 (top panel)). As previously discussed, **L1** alone shows a strong fluorescence and on addition of Pd^{2+} ion there is a considerable quenching in the fluorescence intensity. However, upon addition of EDTA to the same solution the emission intensity got enhanced and peak was identical to that of the probe **L1**. It was noteworthy that EDTA has a better chelating ability with Pd^{2+}, and **L1+** Pd^{2+} complex could be easily detached upon complexation of EDTA with Pd^{2+} i.e., probe **L1** was free from the complex solution [43]. These results indicate that the Pd^{2+} recognition process is completely a reversible one, which can be applied for realistic application. The emission changes were almost reversible even after several cycles with the sequentially addition of Pd^{2+} and EDTA as shown in Figure S9 [44]. Thus, these result indicated that sensor **L1** towards Pd^{2+} could be recyclable simply through using proper reagent such as EDTA. The SEM images of **L1** and **L1**-Pd^{2+} complex are displayed in Figure S10 (a), (b). The morphological changes of **L1** with insertion of Pd^{2+} were analyzed by using SEM analysis. Receptor **L1** shows glassy sheet like structure in the free state. However, on the addition of Pd^{2+} the glassy structure was changed and the complex molecules were agglomerated because of the formation of the **L1**-Pd^{2+} coordination complex, which further confirms the probe **L1** selectivity towards Pd^{2+} ions[45]. The chemical composition of the receptor **L1**-Pd^{2+} ion complex is measured utilizing EDAX analysis (Figure S10 (c),(d)) indicates the presence of carbon (C), nitrogen (N), Sulfur (S) and Palladium (Pd) elements in the receptor **L1**-Pd^{2+} ion complex.

3.8. Density Functional Theory calculations

To further understand the absorption and fluorescence behavior of the probe L1 and L1-Pd^{2+} complex, we carried out DFT calculations with the 6-31G* basis set using the Gaussian 09 program. The optimized structure of probe L1 shows a planar structure. The bond angle -112.44 of N-C-N in probe L1 slightly becomes increased to 114.5 after coordination with Pd^{2+} ion and the charges on the N atom of L1 and L1-Pd^{2+} is found to be -0.572 and -0.464 reveals that the electron density on the N atom is decreased after coordination with Pd^{2+} ion which results in the increased bond angle. The SCF calculations for NMR studies also carried out for L1 and L1-Pd^{2+} ion in TMS HF/6-31G (d) GIAO as a reference. The ^{1}H NMR analysis shows that the aromatic proton (14) shifts to down shield region after coordination with Pd^{2+} ion which further confirms the experimental evidences (Figure S13).

Finally, the above results clearly states that the fluorescence quenching spectral responses of **L1**-Pd^{2+} ion arises primarily due to the paramagnetic nature of the Pd^{2+} ion and the reverse photoinduced electron transfer also plays a role in the quenching effect**.** The 2:1 binding stoichiometry was confirmed by ^{1}H-NMR titration studies, mass spectra, Job's plot and Benesi-Hildebrand equations. Therefore a plausible binding mechanism is proposed as shown in scheme 2.

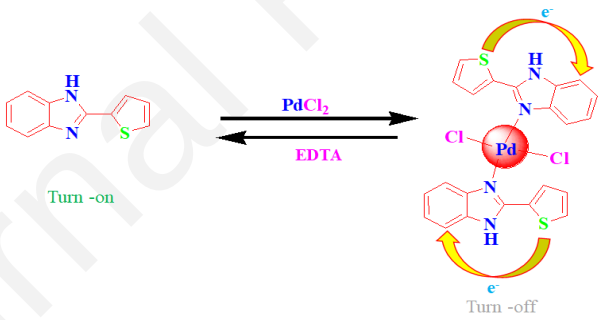

Scheme 2. Proposed binding mechanism of probe **L1** with Pd^{2+} ion

3.9 Biological studies

The results of the antibacterial activity of **L1**, Pd^{2+} ion (palladium), **L1**-Pd^{2+} ion were given in Table 1. DMSO, in which all the compounds were dissolved, did not show any antibacterial activity against *S.aureus*, but it was inhibited by Pd^{2+}, **L1** and **L1**-Pd^{2+} ion complex. Ampicillin also exhibited inhibitory effect on *S.aureus*. Interestingly, against E.coli, **L1** showed

no zone of inhibition whereas the **L1**-Pd^{2+} ion complex showed moderate antibacterial activity (Figure S14). It was also observed that the zone of inhibition for Pd^{2+} and **L1**-Pd^{2+} ion towards *E.coli* was lesser that of *S.aureus*. Overall, the ligand showed better inhibiting activity towards Gram positive bacteria than Gram negative bacteria. Testing against both bacteria, the antibacterial activity of the ligand was increased when complexed with palladium but slightly lower than palladium alone. Our results display the same pattern as showed by Karunaker [46] who showed that there is an increase in antibacterial and antifungal activities of the ligand-palladium complex compared to that of free ligand. Joseyphus and Nair [47] also found that the ligand-palladium complex exert more antibacterial activity than the ligand. They also attributed this phenomenon of toxicity of the complexes to the increased lipophilic nature of the complexes due to chelation. Chelation enhances bactericidal activity of the ligand which may be due to the fact that, the positive charge of the chelated probe **L1**-Pd^{2+} ion is partly shared with donor atoms present in **L1** [48]. There is also a possible explanation for the increased inhibiting activity of the complex as both ligand and the metal ion may interfere in diverse manner during the growth of the microbe [49]. Thus it may possible that the sensor **L1** and their metal probe **L1**-Pd^{2+} ion have the potential to be employed as antibacterial agents in human [50]. The zone of inhibition formed by the ligand and the complex were comparable to that of the standard drug Ampicillin.

Table: 1. *In vitro* anti-bacterial activity of **L1** and **L1**-Pd^{2+} ion

Compound	**Zone of Inhibition (mm in diameter)**	
	Staphylococcus aureus	***Escherichia coli***
$Pd(NO_3)$ ion (Palladium)	20	23
L1	16	No zone
L1-Pd^{2+} ion	18	13
DMSO	No zone	05
Ampicillin	22	24

3.10 Molecular docking studies

High-resolution crystal structures of Staphylococcus aureus methionine aminopeptidase **L1** in **L1**-Pd^{2+} ion with various keto heterocycles and aminoketones are taken for molecular

modeling studies for synthesized 2-(thiophen-2-yl)-1H-benzo[d]imidazole compounds. Methionine aminopeptidases (MetAPs) are ubiquitous enzymes found in both eukaryotic and prokaryotic cells and play a critical role in the maturation of proteins for proper function, targeting, and degradation (Giglione).[51] Based on the above said biological factor *Staphylococcus aureus* methionine amino peptidase I, **L1**-Pd^{2+} ion is targeted protein, we have retrieved from the Protein Data Bank (PDB ID: 1QXY) (Douangamath).[52] The study reveals that the molecules have good binding capability with the active site amino acids of Staphylococcus receptor. In all these complexes, the non-bonded interactions limit is varied from 2.5Å to 3.5Å which reveals that the ligands may result in a strong inhibition. Therefore, it can be concluded that both the size and flexibility play a prominent role in binding with the Staphylococcus enzyme.

The three-dimensional representations of complexes of the Staphylococcus aureus methionine aminopeptidase I complex are shown in (Figure S15&S16). Here two different types of ligands are docked with Staphylococcus aureus methionine amino peptidase I receptor using the program Docking Server. The Ligplot depicts that the compounds (Figure S18 &S19) have similar mode of binding interactions with Staphylococcus protein. The Est. Free Energy of Binding, vdW+Hbond+desolv Energy and Total Inter molec. Energy is calculated for each compound. Both compounds form the best interaction with the active site residues of His 151, which is involved in the key interactions with compounds are strictly conserved residues in targeted protein. Compared to **L1**, **L1**-Pd^{2+} ion have more hydrogen bond interaction and Est. Free Energy of Binding, vdW+Hbond+desolv Energy and Total Inter molec. Energy is more active in the targeted protein. The hydrogen bond interaction of the best compounds with the receptor **L1** molecule is given in (Figure S17) and the energy values were tabulated in Table 2.

Table 2

Hydrogen bond Interaction and docking score of best compounds With the Staphylococcus Targeted Protein

Sl. No	**Ligand Name**	**Est. Free Energy of Binding**	**vdW+Hbond +desolv Energy**	**Total Intermolec. Energy**	**Interactions**	**(distance in Å)**
1	Probe **L1**	-5.34kcal/mol	-5.58kcal/mol	-5.64kcal/mol	N2-HIS151	3.86

2	Probe **L1**-Pd^{2+}	-6.57kcal/mol	-6.71kcal/mol	-6.75kcal/mol	N1-HIS151 N2-HIS151	3.85 3.85

3.11 Bio imaging:

Bio probing assessment of probe **L1** on *Artemia salina* showed clear incidents of cellular uptake. Epifluorescence image of *Artemia salina* showed an excitation in Ex 250-350 nm. Both the intracellular and pheriphral components of *Artemia salina* was observed with complete fluorescence at 370 nm (Figure 12). Specific internal cellular component of fluorescence in *Artemia salina* was reported by Murugase [53]. No fluorescence was observed in the palladium, probe **L1**-Pd^{2+} ion complex and solvents confirms inhibition of fluorescence by palladium. These observations support the interaction of probe **L1** with Pd^{2+} ion in the solvent medium during photometry assessment.

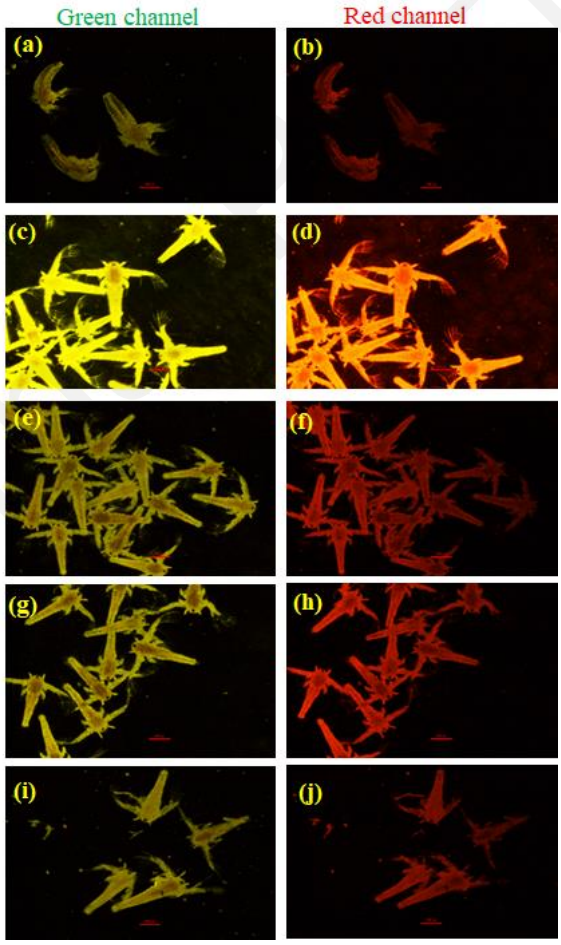

Figure 12. Bioimaging of *Artemia Salina* (a, c, e, g, i) green microscopic images, *Artemia Salina* (b, d, f, h, j) red fluorescence microscopic images. (a) green image of *Artemia Salina* (b) red image of *Artemia Salina,* (c) green field image of probe **L1**(20μM) accumulated to *Artemia Salina,* (d) red field image of probe **L1**(20μM) accumulated to *Artemia Salina* (20μM), (e) green field image of probe **L1**(20μM) and Pd^{2+} (20μM) accumulated to *Artemia Salina* (20μM), (f) red field image of probe **L1**(20μM) and Pd^{2+} (20μM) accumulated to *Artemia Salina* (20μM), (g) green field image of Pd^{2+} (20μM) accumulated to *Artemia Salina* (20μM), (h) red field image of Pd^{2+} (20μM) accumulated to *Artemia Salina* (20μM), (i) green field image of CH_3CN (20μM) accumulated to *Artemia Salina* (20μM), (j) red field image of CH_3CN (20μM) accumulated to *Artemia Salina* (20μM),

4. Conclusion

In summary, a simple reversible chemosensor **L1** for selective detection Pd^{2+} with absorption "off-on" and emission "on-off" signals was achieved compared to other potentially competing meta ions. Both the emission and absorbance spectroscopy delivers information for the creation of 1:2 stoichiometry complexes between Pd^{2+} and **L1**. The association constants and the limit of detection by both the modes have been calculated. The DFT calculations further supports the experimental evidences. Biological applications like antibacterial properties and *in vitro* bio imaging studies on *Artemia salina* has been studied and discussed. Currently, other imidazole based chemosensors and their varied environmental and biological applications are underway in our laboratory.

5. Acknowledgement

This work is supported by the SERB-EMR grant by the DST (Sanction NO.*SERB-EMR/2016/005692)* to RN. Center for research in Nanosciences, KITS, Panjab University – SAIF and The Gandhigram Rural Institute (Deemed to be University) supported the microscopic and spectral details for this work.

References

[1] K.P. Carter, A.M. Young, A.E. Palmer, Fluorescent sensors for measuring metal ions in living systems, Chem. Rev. 114 (2014) 4564–4601. doi:10.1021/cr400546e.

[2] X. Zhang, Y. Xiao, X. Qian, A ratiometric fluorescent probe based on FRET for imaging Hg2+ ions in living cells, Angew. Chemie - Int. Ed. 47 (2008) 8025–8029. doi:10.1002/anie.200803246.

[3] X. Peng, J. Du, J. Fan, J. Wang, Y. Wu, J. Zhao, S. Sun, T. Xu, A selective fluorescent sensor for imaging Cd2+ in living cells, J. Am. Chem. Soc. 129 (2007) 1500–1501. doi:10.1021/ja0643319.

[4] K. Shen, X. Han, G. Xia, X. Lu, Cationic Pd(<scp>ii</scp>)-catalyzed cyclization of N-tosyl-aniline tethered alkynyl ketones initiated by hydropalladation of alkynes: a facile way to 1,2-dihydro or 1,2,3,4-tetrahydroquinoline derivatives, Org. Chem. Front. 2 (2015) 145–149. doi:10.1039/C4QO00286E.

[5] J.G. de Vries, A unifying mechanism for all high-temperature Heck reactions. The role of palladium colloids and anionic species, Dalt. Trans. (2006) 421–429. doi:10.1039/B506276B.

[6] C. Locatelli, D. Melucci, G. Torsi, Determination of platinum-group metals and lead in vegetable environmental bio-monitors by voltammetric and spectroscopic techniques: Critical comparison, Anal. Bioanal. Chem. 382 (2005) 1567–1573. doi:10.1007/s00216-005-3356-4.

[7] J. Cui, D.-P. Li, S.-L. Shen, J.-T. Liu, B.-X. Zhao, A simple and effective fluorescent probe based on rhodamine B for determining Pd 2+ ions in aqueous solution, RSC Adv. 5 (2014) 3875–3880. doi:10.1039/C4RA12649A.

[8] G.O.D. Estrada, A.L.P. Blanco, J.F.M. Da Silva, C.G. Alonso, N.R.C. Fernandes-Machado, L. Cardozo-Filho, R.O.M.A. De Souza, L.S.M. E Miranda, Pd/Nb 2O 5: Efficient supported palladium heterogeneous catalyst in the production of key intermediates for the synthesis of “sartans” via the Suzuki reaction, Tetrahedron Lett. 53 (2012) 1089–1093. doi:10.1016/j.tetlet.2011.12.076.

[9] J. Kielhorn, C. Melber, D. Keller, I. Mangelsdorf, Palladium--a review of exposure and effects to human health., Int. J. Hyg. Environ. Health. 205 (2002) 417–32. doi:10.1078/1438-4639-00180.

[10] Z. Guo, S. Park, J. Yoon, I. Shin, Recent progress in the development of near-infrared fluorescent probes for bioimaging applications, Chem. Soc. Rev. 43 (2014) 16–29. doi:10.1039/C3CS60271K.

[11] X. Li, X. Gao, W. Shi, H. Ma, Design Strategies for Water-Soluble Small Molecular Chromogenic and Fluorogenic Probes, (2012).

[12] K. Van Meel, A. Smekens, M. Behets, P. Kazandjian, R. Van Grieken, Determination of platinum, palladium, and rhodium in automotive catalysts using high-energy secondary target X-ray fluorescence spectrometry, Anal. Chem. 79 (2007) 6383–6389. doi:10.1021/ac070815r.

[13] Z.Y. Xu, J. Li, S. Guan, L. Zhang, C.Z. Dong, Highly selective and sensitive fluorescence chemosensor for the detection of palladium species based on Tsuji-Trost reaction, Spectrochim. Acta - Part A Mol. Biomol. Spectrosc. 148 (2015) 7–11. doi:10.1016/j.saa.2015.03.130.

[14] P. Molina, A. Tárraga, F. Otón, Imidazole derivatives: A comprehensive survey of their recognition properties, Org. Biomol. Chem. 10 (2012) 1711. doi:10.1039/c2ob06808g.

[15] F. Harris, L. Pierpoint, PhotodynamicTherapy Based on 5-Aminolevulinic Acid and Its Use as an Antimicrobial Agent, Med. Res. Rev. 29 (2012) 1292–1327. doi:10.1002/med.

[16] A. Chawla, A. Sharma, A.K. Sharma, Review: A convenient approach for the synthesis of imidazole derivatives using microwaves, Der Pharma Chem. 4 (2012) 116–140.

[17] G.M. Morris, D.S. Goodsell, R.S. Halliday, R. Huey, W.E. Hart, R.K. Belew, A.J. Olson, Automated docking using a Lamarckian genetic algorithm and an empirical binding free energy function, J. Comput. Chem. 19 (1998) 1639–1662. doi:10.1002/(SICI)1096-987X(19981115)19:14<1639::AID-JCC10>3.0.CO;2-B.

[18] F.J. Solis, R.J.-B. Wets, Minimization by Random Search Techniques, Math. Oper. Res. 6 (1981) 19–30. doi:10.1287/moor.6.1.19.

[19] S. Irshad, M. Mahmood, F. Perveen, In-Vitro Anti-Bacterial Activities of Three Medicinal Plants Using Agar Well Diffusion Method, Res. J. Biol. 02 (2012) 1–8.

doi:10.1093/cid/cir240.

[20] L. Boyanova, G. Gergova, R. Nikolov, S. Derejian, E. Lazarova, N. Katsarov, I. Mitov, Z. Krastev, Activity of Bulgarian propolis against 94 Helicobacter pylori strains in vitro by agar-well diffusion, agar dilution and disc diffusion methods, J. Med. Microbiol. 54 (2005) 481–483. doi:10.1099/jmm.0.45880-0.

[21] I.A. Holder, S.T. Boyce, Agar well diffusion assay testing of bacterial susceptibility to various antimicrobials in concentrations non-toxic for human cells in culture, Burns. 20 (1994) 426–429. doi:10.1016/0305-4179(94)90035-3.

[22] Z. Bikadi, E. Hazai, Application of the PM6 semi-empirical method to modeling proteins enhances docking accuracy of AutoDock, J. Cheminform. 1 (2009) 1–16. doi:10.1186/1758-2946-1-15.

[23] R. Martins, N. Fernandez, R. Beiras, V. Vasconcelos, Toxicity assessment of crude and partially purified extracts of marine Synechocystis and Synechococcus cyanobacterial strains in marine invertebrates, Toxicon. 50 (2007) 791–799. doi:10.1016/j.toxicon.2007.06.020.

[24] S. Irshad, M. Mahmood, F. Perveen, In-Vitro Anti-Bacterial Activities of Three Medicinal Plants Using Agar Well Diffusion Method, Res. J. Biol. 02 (2012) 1–8. doi:10.1093/cid/cir240.

[25] S. Santhoshkumar, K. Velmurugan, J. Prabhu, G. Radhakrishnan, R. Nandhakumar, Inorganica Chimica Acta A naphthalene derived Schiff base as a selective fluorescent probe, Inorganica Chim. Acta. 439 (2016) 1–7. doi:10.1016/j.ica.2015.09.030.

[26] L. Wenfeng, M. Hengchang, L. Con, M. Yuan, Q. Chunxuan, Z. Zhonwei, Y. Zengming, C. Haiying, L. Ziqiang, A self-assembled triphenylamine-based fluorescent chemosensor for selective detection of Fe 3+ and Cu 2+ ions in aqueous solution, RSC Adv. 5 (2015) 6869–6878. doi:10.1039/C4RA12025F.

[27] R.M. Duke, E.B. Veale, F.M. Pfeffer, P.E. Kruger, T. Gunnlaugsson, Colorimetric and fluorescent anion sensors: an overview of recent developments in the use of 1,8-

naphthalimide-based chemosensors, Chem. Soc. Rev. 39 (2010) 3936. doi:10.1039/b910560n.

[28] P. Jin, C. Jiao, Z. Guo, Y. He, S. Zhu, H. Tian, W. Zhu, Rational design of a turn-on fluorescent sensor for α-ketoglutaric acid in a microfluidic chip, Chem. Sci. 5 (2014) 4012–4016. doi:10.1039/C4SC01378F.

[29] P. Kumar, V. Kumar, R. Gupta, Selective fluorescent turn-off sensing of Pd^{2+} ion: applications as paper strips, polystyrene films, and in cell imaging, RSC Adv. 7 (2017) 7734–7741. doi:10.1039/C6RA27565F.

[30] K. Wechakorn, S. Prabpai, K. Suksen, P. Kanjanasirirat, Y. Pewkliang, S. Borwornpinyo, P. Kongsaeree, A rhodamine-triazole fluorescent chemodosimeter for Cu2+detection and its application in bioimaging, Luminescence. 33 (2018) 64–70. doi:10.1002/bio.3373.

[31] C. Wu, C. Wang, Q. Zhu, X. Zeng, C. Redshaw, T. Yamato, Sensors and Actuators B : Chemical Click synthesis of a quinoline-functionalized hexahomotrioxacalix [3] arene : A turn-on fluorescence chemosensor for Fe 3 +, Sensors Actuators B. Chem. 254 (2018) 52–58. doi:10.1016/j.snb.2017.07.048.

[32] J. Prabhu, K. Velmurugan, R. Nandhakumar, Spectrochimica Acta Part A : Molecular and Biomolecular Spectroscopy Development of fluorescent lead II sensor based on an anthracene derived chalcone, Spectrochim. ACTA PART A Mol. Biomol. Spectrosc. 144 (2015) 23–28. doi:10.1016/j.saa.2015.02.028.

[33] B. Liu, Y. Bao, F. Du, H. Wang, J. Tian, R. Bai, Synthesis and characterization of a fluorescent polymer containing 2,6-bis(2-thienyl)pyridine moieties as a highly efficient sensor for Pd2+detection, Chem. Commun. 47 (2011) 1731–1733. doi:10.1039/c0cc03819a.

[34] M.S. Kim, S.Y. Lee, J.M. Jung, C. Kim, A new Schiff-base chemosensor for selective detection of Cu2+and Co2+and its copper complex for colorimetric sensing of S2-in aqueous solution, Photochem. Photobiol. Sci. 16 (2017) 1677–1689. doi:10.1039/c7pp00229g.

[35] C. Ram, S. Sivamani, T. Micha Premkumar, V. Hariram, Computational study of leading edge jet impingement cooling with a conical converging hole for blade cooling, ARPN J. Eng. Appl. Sci. 12 (2017) 6397–6406. doi:10.1039/b000000x.

[36] Q. Zeng, P. Cai, Z. Li, J. Qin, B.Z. Tang, An imidazole-functionalized polyacetylene: Convenient synthesis and selective chemosensor for metal ions and cyanide, Chem. Commun. (2008) 1094–1096. doi:10.1039/b717764j.

[37] K. Li, X. Su, Y. Wang, F. Tao, Y. Cui, H. Zhang, T. Li, D-π-A type barbituric derivatives: Aggregation induced emission, mechanofluorochromic and solvatochromic properties, J. Lumin. 203 (2018) 50–58. doi:10.1016/j.jlumin.2018.06.025.

[38] C. Ma, Y.Q. Ou, C.T.L. Chan, A.K.W. Wong, R.C.T. Chan, B.P.Y. Chung, C. Jiang, M.L. Wang, W.M. Kwok, Nonradiative dynamics determined by charge transfer induced hydrogen bonding: A combined femtosecond time-resolved fluorescence and density functional theoretical study of methyl dimethylaminobenzoate in water, Phys. Chem. Chem. Phys. 20 (2018) 1240–1251. doi:10.1039/c7cp05140a.

[39] P. Mazumdar, S. Maity, M. Shyamal, D. Das, G.P. Sahoo, A. Misra, Proton triggered emission and selective sensing of picric acid by the fluorescent aggregates of 6,7-dimethyl-2,3-bis-(2-pyridyl)-quinoxaline, Phys. Chem. Chem. Phys. 18 (2016) 7055–7067. doi:10.1039/c5cp05827a.

[40] G. Kasirajan, V. Krishnaswamy, N. Raju, M. Mahalingam, M. Sadasivam, M. Palathurai Subramaniam, S. Ramasamy, New pyrazolo-quinoline scaffold as a reversible colorimetric fluorescent probe for selective detection of Zn2+ions and its imaging in live cells, J. Photochem. Photobiol. A Chem. 341 (2017) 136–145. doi:10.1016/j.jphotochem.2017.03.035.

[41] J. Prabhu, K. Velmurugan, Q. Zhang, S. Radhakrishnan, L. Tang, R. Nandhakumar, Symmetric fluorescent probes for the selective recognition of Ag-ion via restricted C=N isomerization and on-site visual sensing applications, J. Photochem. Photobiol. A Chem. 337 (2017) 6–18. doi:10.1016/j.jphotochem.2017.01.006.

[42] K. Velmurugan, A. Thamilselvan, R. Antony, V.R. Kannan, L. Tang, R. Nandhakumar,

Imidazoloquinoline bearing thiol probe as fluorescent electrochemical sensing of Ag and relay recognition of Proline, J. Photochem. Photobiol. A Chem. 333 (2017) 130–141. doi:10.1016/j.jphotochem.2016.10.025.

[43] A. V. Sakharutov, Hydrostatic pressing in making components for cryogenic pipelines, Chem. Pet. Eng. 26 (1990) 238–241. doi:10.1007/BF01149680.

[44] J.M. Lázaro Martínez, P.N. Romasanta, A.K. Chattah, G.Y. Buldain, NMR characterization of hydrate and aldehyde forms of imidazole-2- carboxaldehyde and derivatives, J. Org. Chem. 75 (2010) 3208–3213. doi:10.1021/jo902588s.

[45] D.S. Ermolat'ev, E. V. Van Der Eycken, A divergent synthesis of substituted 2-aminoimidazoles from 2-aminopyrimidines, J. Org. Chem. 73 (2008) 6691–6697. doi:10.1021/jo8008758.

[46] Y. Zhu, H. Li, B. Shi, W. Qu, Y. Zhang, Q. Lin, H. Yao, T. Wei, RSC Advances A reversible fl uorescent chemosensor for the rapid detection of mercury ions (II) in water with high sensitivity and selectivity †, RSC Adv. 4 (2014) 61320–61323. doi:10.1039/C4RA09961C.

[47] Y. Long, J. Zhou, M. Yang, B. Yang, Original article A selective and sensitive off – on probe for palladium and its application for living cell imaging, 27 (2016) 205–210.

[48] S. Suresh, N. Bhuvanesh, J. Prabhu, A. Thamilselvan, R.J.R. S., K. Kannan, R.K. V., R. Nandhakumar, Pyrene based chalcone as a reversible fluorescent chemosensor for Al3+ion and its biological applications, J. Photochem. Photobiol. A Chem. 359 (2018) 172–182. doi:10.1016/j.jphotochem.2018.04.009.

[49] D. Karunaker, T. Baskara Rao, B. Srinivas, A. Mallikarjun, M. Ashok, Synthesis and antimicrobial activities of new Schiff's base and metal complexes derived from imidazole, Der Pharm. Lett. 8 (2016) 79–83.

[50] M. Sunitha, P. Jogi, B. Ushaiah, C.G. Kumari, Synthesis, characterization and antimicrobial activity of transition metal complexes of Schiff base ligand derived from 3-ethoxy salicylaldehyde and 2-(2-aminophenyl) 1-H-benzimidazole, E-Journal Chem. 9

(2012) 2516–2523. doi:10.1155/2012/287909.

[51] R. Selwin Joseyphus, C. Shiju, J. Joseph, C. Justin Dhanaraj, K.C. Bright, Synthesis and characterization of Schiff base metal complexes derived from imidazole-2-carboxaldehyde with L-phenylalanine, Der Pharma Chem. 7 (2015) 265–270. doi:10.1016/j.saa.2014.05.050.

[52] J. Travis, J. Potempa, Bacterial proteinases as targets for the development of second-generation antibiotics, Biochim. Biophys. Acta - Protein Struct. Mol. Enzymol. 1477 (2000) 35–50. doi:10.1016/S0167-4838(99)00278-2.

[53] M. Gomleksiz, C. Alkan, B. Erdem, Synthesis , Characterization and Antibacterial Activity of Imidazole Derivatives of 1 , 10-Phenanthroline and their Cu (II), Co (II) and Ni (II) Complexes, (2013) 107–112.